Thermionic emission and Frank-Hertz oscillations

Matthew Krupcale, Evan Telford
Department of Physics, Case Western Reserve University, Cleveland Ohio, 44106-7079
21 October 2012

Abstract

Charges emitted from a surface through thermionic emission have a current density that depends on the temperature of the material and its work function. Using thermionic emission, the work function for a tungsten filament was found from a linear fit to be $e\phi = 3.13 \pm 0.05$ eV, in disagreement with the expected value of 4.5 eV. When electrons were emitted and accelerated from the cathode of a vacuum tube filed with mercury atom scattering centers, a periodicity was observed in the anode *I-V* characteristic, indicative of the excitation of mercury at discrete energies of $E_{\text{ex}} = 4.77 \pm 0.05$ eV. This result disagrees with the theoretical value of $\Delta E = 4.89$ eV, corresponding to the excitation energy of mercury observed in the Frank-Hertz experiment. Using the excitation energy of mercury and the accelerating potential at the first oscillation, the contact potential difference between the anode and cathode materials was found to be $V_c = 1.9 \pm 0.1$ V.

Introduction

The objectives of this experiment are to determine the work function of a tungsten filament and to measure the excitation energy of the mercury atom. The thermionic emission of electrons from a tungsten filament in a vacuum tube was examined in order to determine the work function of tungsten. In the saturation region of the anode *I-V* characteristic, the anode current should be constant as a function of potential and should depend only on the filament temperature and work function according to the Richardson-Dushman equation; fitting measured currents and temperatures to this curve will yield the work function. When the vacuum tube is

filled with mercury vapor, however, the electrons can scatter off of the mercury atoms in a completely inelastic collision and excite the mercury at discrete energies. This periodic excitation results in an oscillatory anode *I-V* characteristic, and the periodicity can be used to directly measure the excitation energy of mercury.

Theory

Thermionic Emission

In an electron vacuum tube, as the anode potential becomes sufficiently large so that the filament is no longer space charge limited, the anode current depends only on the filament temperature and surface area. In this saturation region of the *I-V* characteristic, the anode current is independent of the anode potential. This leads to the Richardson-Dushman equation [1,2]

$$J = AT^2 e^{-\frac{e\phi}{kT}} \tag{1}$$

where J is the emission current per unit area of the metal surface, and A is a material-dependent constant, T is the absolute temperature, k is Boltzmann's constant, e is the elementary charge, and ϕ is the potential function of the metal. The quantity $e\phi$ is the work function of the metal [2]. As the cathode temperature increases, the saturation current increases.

Frank-Hertz Oscillations and Contact Potential

Introducing an elastic scattering center into the electron tube, such as mercury atoms, which are significantly more massive than electrons, will cause electrons to scatter before reaching the anode, reducing the total anode current. Provided that the accelerating potential between the anode and cathode of the electron tube is less than the excitation energy, the electrons will elastically scatter. When the accelerating potential reaches the level required to excite the mercury atom from the $^1S_0$ ground state to the $^3P_1$ state [3], corresponding to an energy of $\Delta E = 4.89\ \text{eV}$, the scattering becomes inelastic, and the electron loses its kinetic

energy to excite the mercury atom. This inelastic scattering at the excitation energy causes a drop in the anode current. Raising the anode potential further will then cause the excitation to move towards the cathode, allowing the electrons to be re-accelerated, increasing the anode current. If the accelerating potential is sufficiently large, electrons may then experience multiple inelastic collisions with the mercury, resulting in an oscillatory anode *I*-*V* characteristic; this periodicity is direct evidence for a discrete energy level of the mercury atom.

Two dissimilar metals used as electrodes have a contact potential difference given by [4]

$$V_c = \phi_A - \phi_C = V - V_m \tag{2}$$

where ϕ_A and ϕ_C are the potential functions of the anode and cathode, respectively, V is the applied voltage, and V_m is the measured accelerating potential. Then applied voltage at the nth peak is related to the excitation energy and the contact potential according to

$$V_n = nV_{\text{ex}} + V_c = n\left(\frac{E_{\text{ex}}}{e}\right) + V_c \tag{3}$$

where V_{ex} is the excitation potential, E_{ex} is the excitation energy, and e is the elementary charge.

Apparatus and Methods

Thermionic Emission

Thermionic emission was tested using a Leybold Didactic diode P, a high-vacuum tube containing a cathode plate, cathode filament and anode, as shown in Figure 1A. The anode current was measured by a Keithley 487 picoammeter connected in series to the Keithley 487 voltage source by a triaxial cable with alligator clips. The alligator clip connection may not have been ideal for such a precise measurement, but the magnitude of the saturation currents were such that noise was not too problematic. An IGOR Pro script was used to control the Keithley picoammeter and voltage source as well as record the current and voltage measurements. The circuit schematic for the thermionic emission experiment is shown in Figure 1B. The Agilent

E3610A power supply was used to supply current to the cathode filament, ranging from 1.50A to 2.00A in increments of 0.05A. For each filament current, the IGOR Pro script would produce the anode *I-V* characteristic up to 250V, and the filament temperature was measured using an optical pyrometer. Due to the imprecise nature of this qualitative color comparison, the uncertainty in the temperature is one of the largest sources of error.

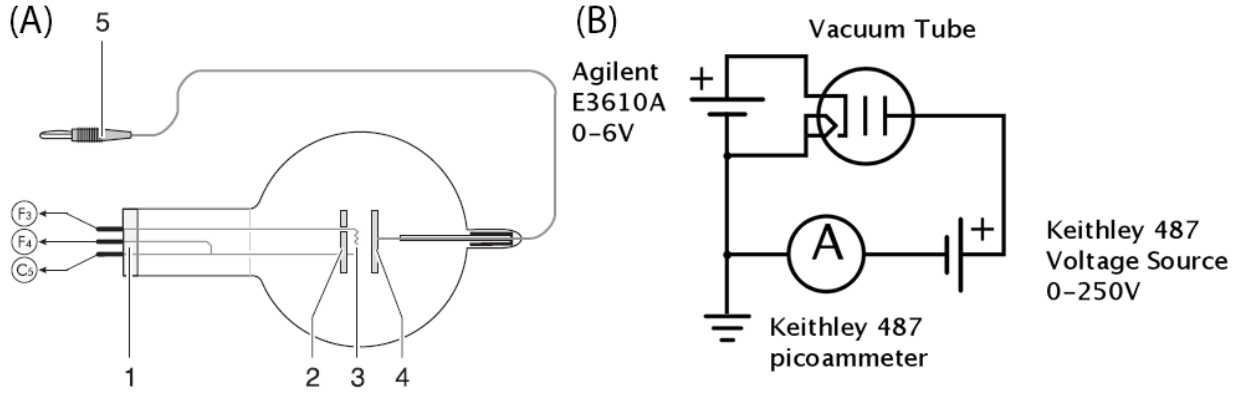

Figure 1 Thermionic emission vacuum tube. (A) Vacuum tube with 1. Pin socket, 2. Cathode plate, 3. Cathode filament (directly heated), 4. Anode, 5. Anode connecting lead; (B) the anode potential is controlled by the Keithley 487 voltage source, and the anode current is measured by the Keithley 487 picoammeter. The filament current is controlled by the Agilent power supply.

Frank-Hertz Oscillations and Contact Potential

The Frank-Hertz experiment was conducted using a three-electrode vacuum tube with a cathode, grid anode and collector electrode. The collector was connected in series with the Keithley 487 picoammeter, and an Agilent E3610A power supply was used to control the collector or bias voltage (see Figure 2). A bias voltage of around 2 to 3V was used for taking measurements, but it was varied from -7 to 7V for testing purposes. A second Agilent power supply controlled the filament current, which was typically about 0.13A but ranged from 0.10A to 0.20A, depending on the vacuum tube temperature. The vacuum tube was contained within a temperature-controlled oven to regulate the vapor pressure of the mercury. The form of the anode *I-V* characteristic also depends on the oven temperature for reasons relating to the mean

free path of the electrons. A thermometer was used to monitor the oven temperature, which was controlled using a variable autotransformer, or variac, and was typically in the range of 180℃ to 200℃. As in the thermionic emission test, the *I-V* characteristics were collected using an IGOR Pro script.

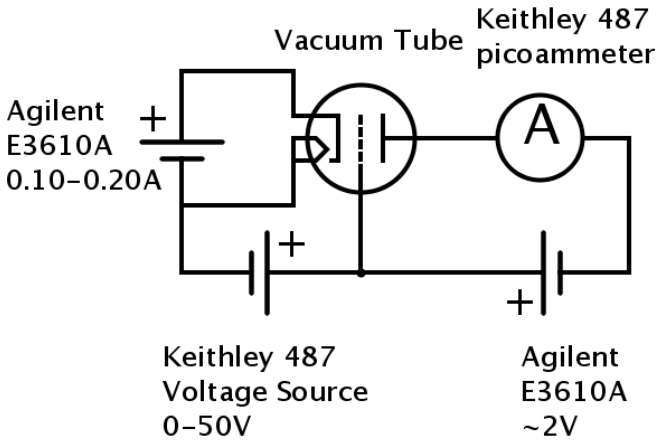

Figure 2 Schematic of Frank-Hertz experiment setup. The anode potential is controlled by the Keithley 487 voltage source, and the anode or collector current is measured by the Keithley 487 picoammeter. The filament current is controlled by the Agilent power supply, and a second power supply controls the collector or bias voltage.

Results and Analysis

Thermionic Emission

The current collected in the anode is proportional to Eq. 1, since the current depends on factors such as the surface area of the filament and the distance between the cathode and anode, both of which are held constant. Then $i \propto J$, so

$$i = \alpha T^2 e^{-\frac{e\phi}{kT}} \tag{4}$$

where i is the anode saturation current, and α is a proportionality factor that has absorbed the constant A. Eq. 4 can be linearized with respect to ϕ by plotting $\ln\left(\frac{i}{T^2}\right)$ versus $\frac{1}{T}$:

$$\ln\left(\frac{i}{T^2}\right) = \ln\alpha - \frac{e\phi}{k}\left(\frac{1}{T}\right) \tag{5}$$

Thus, the work function can be found by either doing a direct, nonlinear fit to Eq. 4, or by doing a linear fit to Eq. 5. The work function in Eq. 5 will then be given by $e\phi = -k(\text{slope})$, where the slope is the linear fit parameter.

The saturation currents were calculated from the average of the currents for which the voltage was greater than the minimum saturation voltage of $V_{\text{sat}} = 100\,\text{V}$ in the anode *I-V* characteristic. The minimum filament current for which the emission current was usable for the calculation of the work function was $I_F = 1.55\text{A}$ since this saturation current at $I_F = 1.50\text{A}$ was nearly three orders of magnitude less than the saturation current at $I_F = 1.55\,\text{A}$, while typical saturation currents increased by less than a single order of magnitude for each $0.05\,\text{A}$ filament current increment. Thus, the point for which $I_F = 1.50\text{A}$ was discarded from the calculation of the work function. Any currents below $I_F = 1.55\text{A}$ produced *I-V* characteristics that contained too much noise, as shown in Figure 3; the *I-V* characteristics above 1.55A are shown in Figure 4.

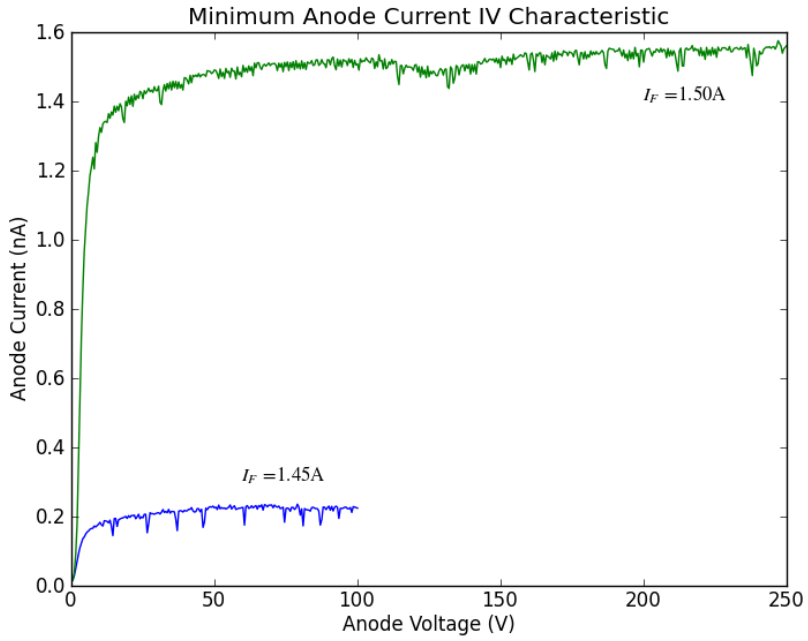

Figure 3 Minimum usable anode currents for work function calculation. Anode currents for which the filament current was less than $I_F = 1.55\text{A}$ were not used in the calculation of the work function.

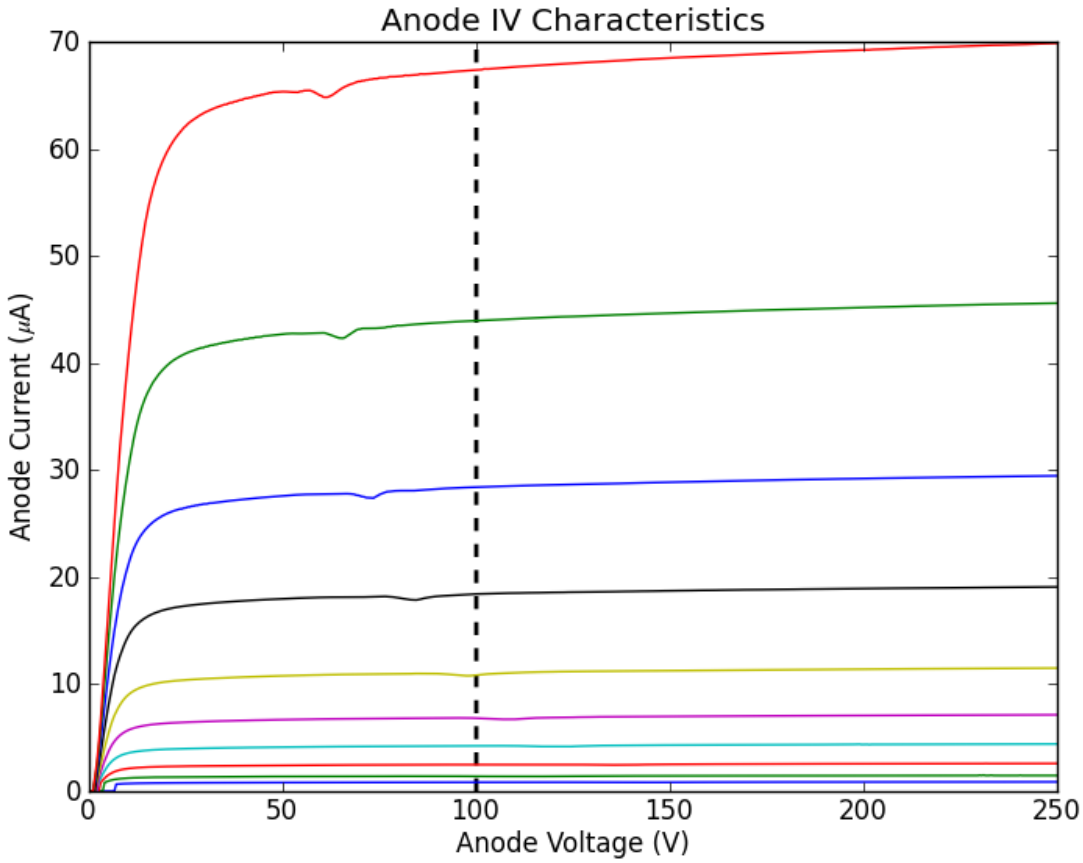

Figure 4 Anode *I-V* Characteristics. The anode potential was raised up to 250V in 0.5V increments. Anode current saturation occurs in all curves by about 100V, as indicated by the dashed vertical line. Curves with higher saturation current are given by higher filament temperatures.

Measurement of the filament brightness temperature were made on two separate occasions by different people using the optical pyrometer, and the true temperature was calculated according to [5]

$$\frac{1}{T} - \frac{1}{T_s} = \frac{k\lambda}{hc} \ln \varepsilon_\lambda \tag{6}$$

where T is the true temperature, T_s is the brightness temperature, h is Planck's constant, c is the speed of light, and ε_λ is the spectral emissivity corresponding to wavelength λ. In the temperature range of interest, the emissivity is approximately $\varepsilon_\lambda = 0.44$ for a wavelength of 645 nm, corresponding to an optical pyrometer effective wavelength [5].

The uncertainties in the current measurements are small compared to the uncertainties in the temperatures because the Keithley 487 picoammeter has accuracies on the order of nanoamps, while the temperature measurements have errors of roughly 30 to 60 Kelvin. Temperature uncertainties were estimated by finding the deviation in the optical pyrometer brightness that was noticeable to the user. The temperature measurement also introduces systematic error, since the deviation of one temperature measurement will inherently affect subsequent measurements in a similar way. For typical saturation currents on the order of microamps, the relative uncertainties are on the order of 10^{-4}, whereas typical temperature measurements have relative uncertainties of roughly one to two percent. The results of these calculations are summarized in Table 1.

Table 1 Thermionic emission currents and filament temperatures. The emission or anode saturation current was determined as a function of filament or cathode temperature. The true temperature is the corrected temperature obtained by Eq. 6 in terms of the brightness temperature, which was measured on two ocassions.

Cathode current, I_F (A)	Anode current, I_A (μA)	True temperature, T (K)	
		Measurement 1	Measurement 2
1.55A	0.86021 ± 0.00009	1570 ± 30	1730 ± 60
1.60A	1.4473 ± 0.0001	1620 ± 30	1750 ± 30
1.65A	2.5436 ± 0.0003	1670 ± 30	1780 ± 50
1.70A	4.3291 ± 0.0004	1700 ± 30	1840 ± 60
1.75A	7.0120 ± 0.0005	1740 ± 30	1850 ± 30
1.80A	11.3141 ± 0.0008	1770 ± 30	1910 ± 50
1.85A	18.881 ± 0.001	1810 ± 30	1960 ± 60
1.90A	29.009 ± 0.003	1850 ± 30	2010 ± 60
1.95A	44.884 ± 0.004	1860 ± 30	2070 ± 60
2.00A	68.794 ± 0.005	1910 ± 30	2160 ± 60

After performing both a nonlinear curve fit to Eq. 4 and a linear fit to Eq. 5 (shown in Figures 5 and 6), using each temperature measurement and the average temperature, the work functions are found using the fit parameters and are summarized in Table 2.

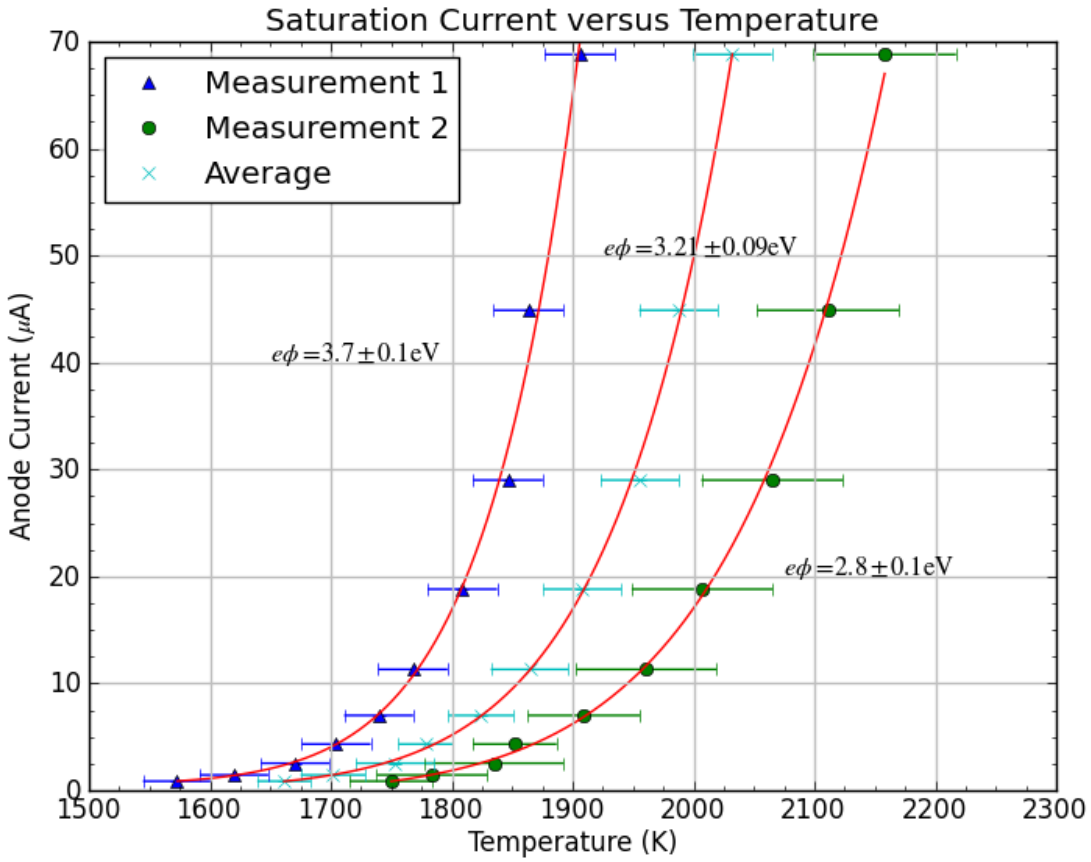

Figure 5 Nonlinear curve fit of the Richardson-Dushman equation. The two separate measurements of the filament temperature and the average temperature are plotted together. Their respective nonlinear curve fits (indicated by the red curves) and work function fit parameter are also shown.

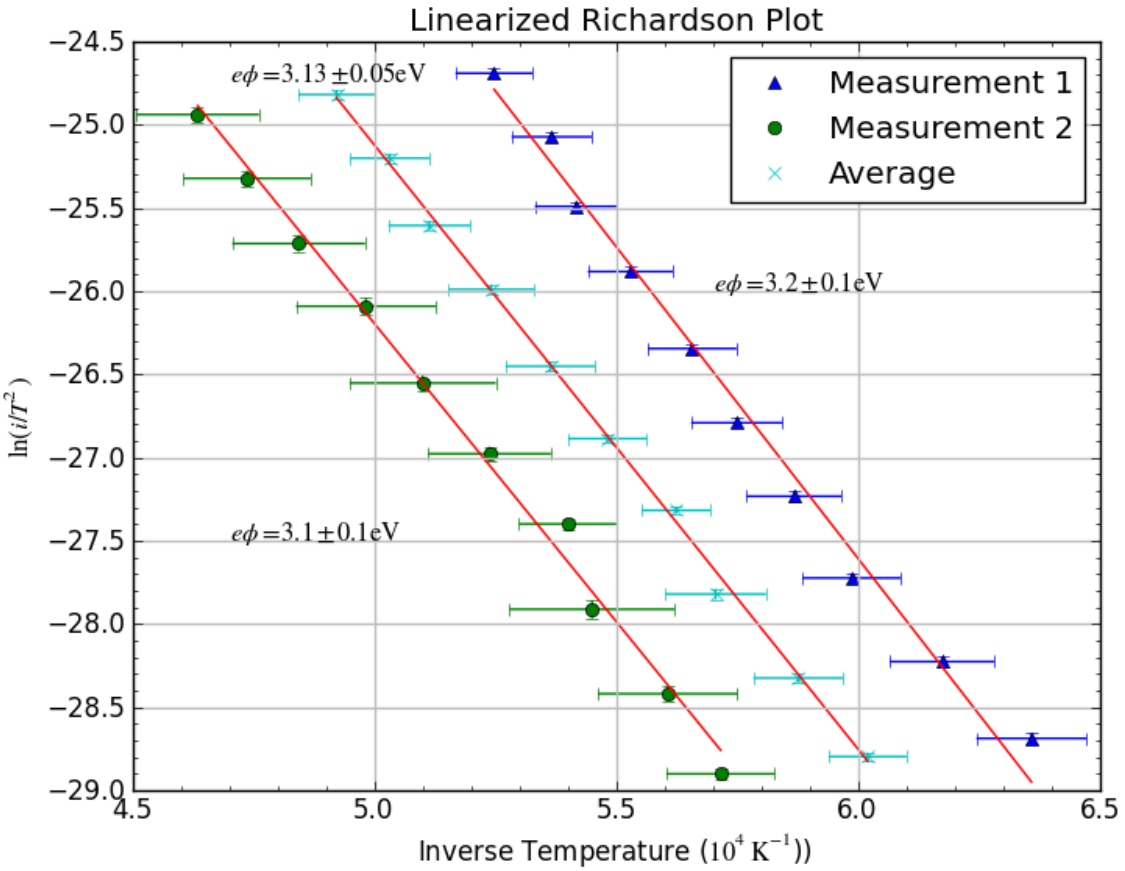

Figure 6 Linear fit of the Eq. 5. The two separate measurements of the filament temperature and the average temperature are plotted together. Their respective linear fits (indicated by the red curves) and work function fit parameter are also shown.

Table 2 Summary of work function results. The work functions for each temperature measurement and the average temperature along with the method used to calculate them.

Fit Method	Work function, $e\phi$ (eV) Temperature Measurement 1	Temperature Measurement 2	Average Temperature
Nonlinear ordinary least-squares	3.7 ± 0.1	2.8 ± 0.1	3.21 ± 0.09
Linear ordinary least-squares	3.2 ± 0.1	3.1 ± 0.1	3.13 ± 0.05

The reduced chi-squared values were calculated for each fit, and the nonlinear fit reduced chi-squared values were all on the order of 10^5 to 10^6, while the reduced chi-squared values for the linear fits were from 4.9 up to 24.5. The high nonlinear fit chi-squared values are most likely

due to the very small uncertainties in the anode currents; on the other hand, the uncertainty in the linear fit dependent variable incorporates uncertainty in the temperature, which was the largest source of error.

Frank-Hertz Oscillations and Contact Potential

The excitation energy of the mercury atom from the ground state is given by Eq. 3 according to

$$V_{n+1} - V_n = (n+1)V_{\text{ex}} + V_c - nV_{\text{ex}} + V_c = V_{\text{ex}} = \frac{\Delta E}{e} \Rightarrow \Delta E = e(V_{n+1} - V_n) \qquad (7)$$

Thus, the contact potential drops out, and the excitation energy can be calculated directly from the difference in applied voltages between subsequent peaks. The uncertainty in this calculation results from uncertainties in the voltage of the maxima or minima of the oscillation. In the voltage range of the oscillations (between roughly $V = 10\text{V}$ and $V = 50\text{V}$), the Keithley 487 voltage source has a maximum accuracy of about $54\ \text{mV}$ for a relative uncertainty of about 0.1 percent. This uncertainty in the Keithley voltage is typically about 20% of the voltage step sizes ($\Delta V = 250\ \text{mV}$) and does not exceed the step sizes, so the limiting factor in our voltage precision is the step size. A sample Frank-Hertz oscillation is shown in Figure 7.

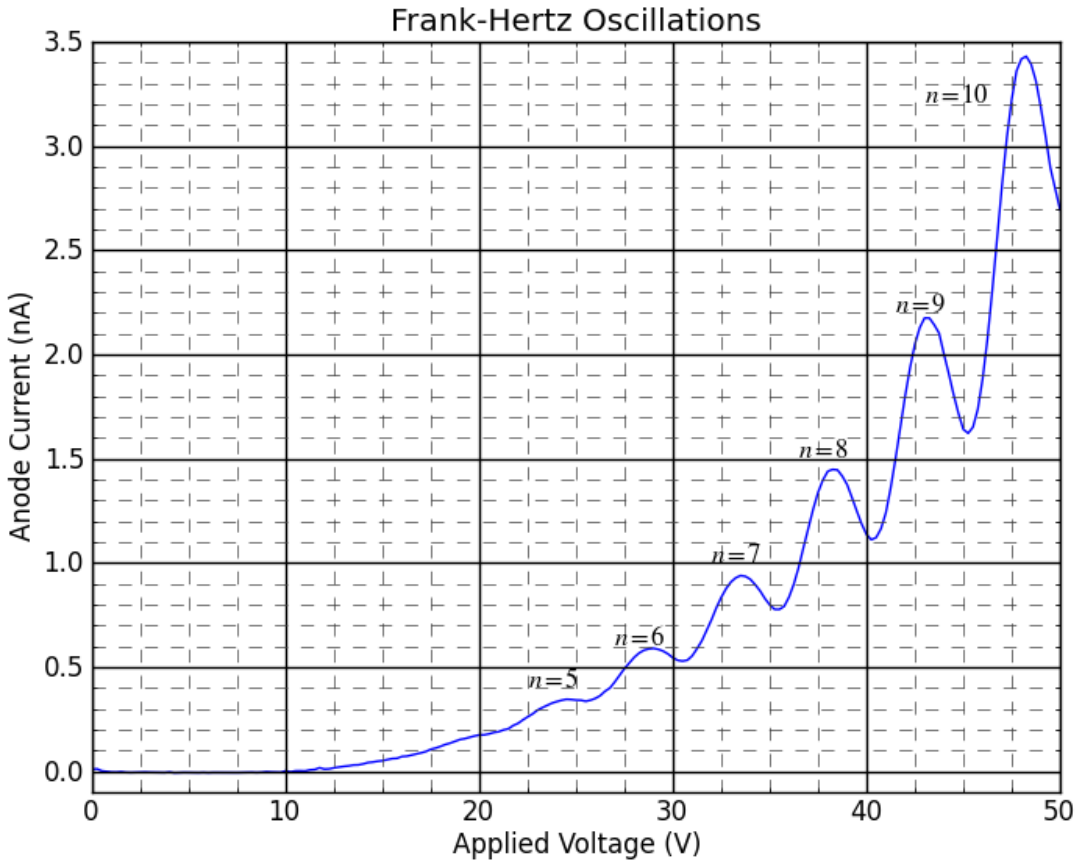

Figure 7 Sample Frank-Hertz Oscillation. This anode *I-V* characteristic displays the oscillations that give evidence for discrete energy levels of the mercury atom. The ***n***th peaks are labeled as shown. This measurement was taken at 205℃ with a +3.0V bias and 130 mA filament current.

Table 3 shows the calculated periods of each of the Frank-Hertz oscillation curves at each peak.

Table 3 Frank-Hertz Oscillation Periods. The differences in peak maxima were calculated between each available peak for various bias or retardation voltages between the grid anode and collector. Measurements were carried out with a filament current of 130 mA at a temperature of 200 to 205℃. Peaks that were not distringuishable were not included.

Bias Voltage	$V_{n+1} - V_n$ (V) for peak n				
	$n = 5$	$n = 6$	$n = 7$	$n = 8$	$n = 9$
-3.0 V		4.6 ± 0.3	4.6 ± 0.3	4.8 ± 0.3	5.2 ± 0.3
		4.80 ± 0.07	4.40 ± 0.07	5.10 ± 0.07	5.10 ± 0.07
$+2.0$ V	4.3 ± 0.4	4.5 ± 0.4	4.8 ± 0.4	5.0 ± 0.4	5.0 ± 0.4
	4.3 ± 0.4	4.8 ± 0.4	5.0 ± 0.4	5.0 ± 0.4	
$+3.0$ V	4.8 ± 0.4	4.5 ± 0.4	4.8 ± 0.4	5.0 ± 0.4	5.0 ± 0.4
	4.3 ± 0.4	4.8 ± 0.4	4.8 ± 0.4	4.8 ± 0.4	5.3 ± 0.4
	4.5 ± 0.4	4.5 ± 0.4	4.8 ± 0.4	4.8 ± 0.4	5.3 ± 0.4
	4.8 ± 0.4	4.5 ± 0.4	4.8 ± 0.4	5.0 ± 0.4	5.0 ± 0.4
	4.3 ± 0.4	4.8 ± 0.4	4.8 ± 0.4	4.8 ± 0.4	5.3 ± 0.4
		4.5 ± 0.7	5.0 ± 0.7	5.0 ± 0.7	5.0 ± 0.7
		4.3 ± 0.4	5.0 ± 0.4	4.5 ± 0.4	5.0 ± 0.4
		4.8 ± 0.4	4.8 ± 0.4	5.0 ± 0.4	5.0 ± 0.4
		4.5 ± 0.4	5.0 ± 0.4	4.8 ± 0.4	5.0 ± 0.4
		4.5 ± 0.4	4.8 ± 0.4	5.0 ± 0.4	5.0 ± 0.4
		4.5 ± 0.4	4.8 ± 0.4	4.8 ± 0.4	5.0 ± 0.4
		4.3 ± 0.4	5.0 ± 0.4	4.8 ± 0.4	5.3 ± 0.4
		4.5 ± 0.4	4.8 ± 0.4	4.8 ± 0.4	5.3 ± 0.4
		4.5 ± 0.4	4.8 ± 0.4	4.8 ± 0.4	5.3 ± 0.4
		4.3 ± 0.4	5.3 ± 0.4	5.0 ± 0.4	4.8 ± 0.4
		4.5 ± 0.4	4.8 ± 0.4	5.0 ± 0.4	5.0 ± 0.4
			4.8 ± 0.4	4.8 ± 0.4	5.3 ± 0.4
			4.8 ± 0.4	4.8 ± 0.4	5.3 ± 0.4
			4.8 ± 0.4	5.0 ± 0.4	5.0 ± 0.4
			4.8 ± 0.4	4.8 ± 0.4	5.3 ± 0.4
			4.8 ± 0.4	5.0 ± 0.4	4.5 ± 0.4
			4.8 ± 0.4	4.8 ± 0.4	5.0 ± 0.4
Average	4.5 ± 0.2	4.55 ± 0.09	4.83 ± 0.08	4.88 ± 0.08	5.09 ± 0.08

Finally, the average over all peaks and all *I-V* characteristics is $E_{\text{ex}} = 4.77 \pm 0.05$ eV. The contact potential difference can also find using Eq. 3 in the form $V_c = V_n - nV_{\text{ex}}$. The applied voltage is $V_n = 6.7 \pm 0.1$ V at the $n = 1$ maximum (see Figure 8), so using the excitation potential $V_{\text{ex}} = 4.77 \pm 0.05$ V, the contact potential is $V_c = 1.9 \pm 0.1$ V.

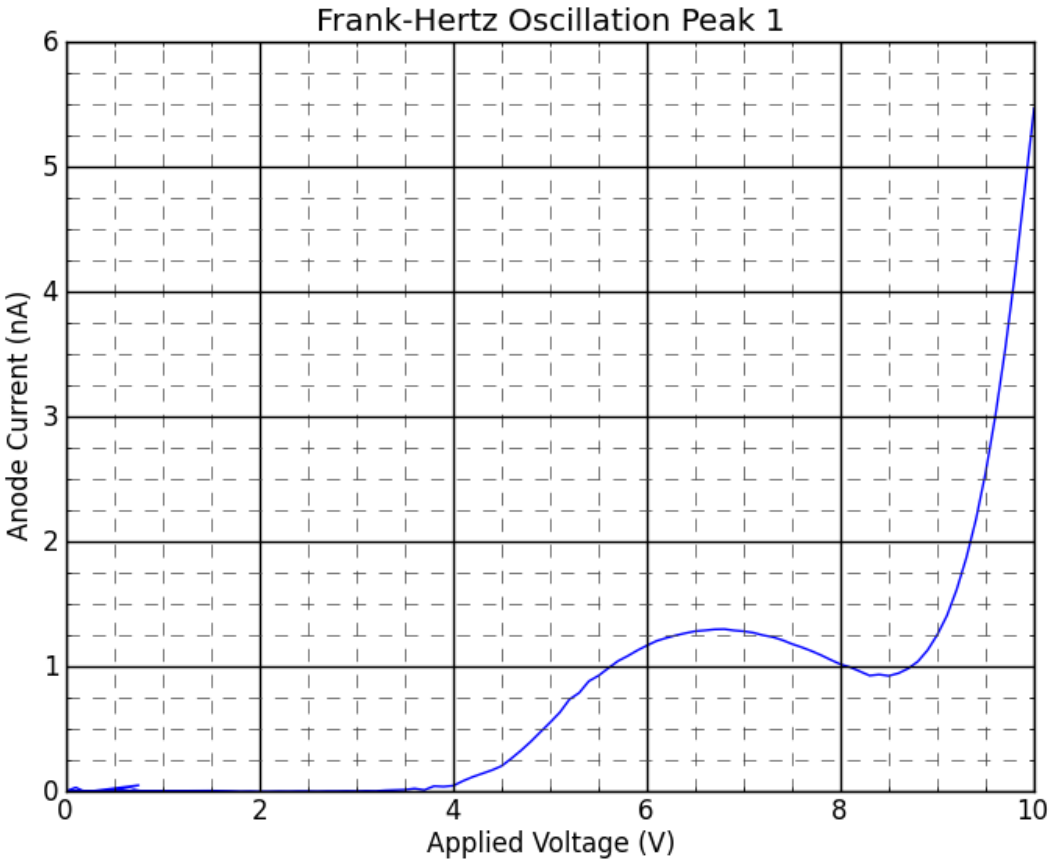

Figure 8 Frank-Hertz Oscillation Peak 1. The first observed peak, corresponding to a single excitation of mercury by electrons, was obtained using low temperatures and low bias voltages to allow the electrons to more easily reach the collector with a small accelerating potential.

Discussion and Conclusions

Thermionic Emission

The theoretical value for the work function of a tungsten filament is 4.5 eV, but can vary as much as 4.32 to 5.22 eV, depending on factors such as crystal orientation [6]. Since the reduced chi-squared values for the nonlinear fits were significantly greater than one, the values of the work function found using the nonlinear least-squares curve fit may be inaccurate. Thus, the linear least-squares regression should have more accurate work function estimates. The linear fit with the smallest reduced chi-squared was obtained by fitting the average temperature values,

and the resulting work function from this fit was found to be $e\phi = 3.13 \pm 0.05$ eV. This value is in disagreement with the theoretical value of 4.5 eV for a typical filament, since it is not within the uncertainty of the work function.

Most of the uncertainty in the measurements and calculation of the work function results from the temperature, which in both Eq. 4 and 5 is in the independent variable, making an ordinary least-squares (OLS) approach inferior to an orthogonal distance regression (ODR). The dependent variables in Eq. 4 and 5 have very little uncertainty compared to the independent variables—temperature and inverse temperature—as can be seen by Figures 5 and 6, and the uncertainty in the independent variable gets lost by the OLS method. Thus, to account for the uncertainty in the independent variable, an ODR fit method would be more appropriate and would propagate the error to the fit parameter more appropriately. Then the work function fit parameter may become more accurate while sacrificing some precision by using an ODR method.

Frank-Hertz Oscillations and Contact Potential

The excitation energy of $\Delta E = 4.89$ eV is not within the uncertainty of the averaged excitation energy $E_{\text{ex}} = 4.77 \pm 0.05$ eV, but it is within the uncertainty of the $n = 7$ and $n = 8$ peaks with energies of 4.83 ± 0.08 eV and 4.88 ± 0.08 eV, respectively. The $n = 5, 6, 9$ peaks are not within their uncertainties of the expected excitation energy, though. A possible explanation for this discrepancy is given by Rapior *et al*. [7], where they show that the spacing between minima increases linearly with minimum order n, due to the larger electron energy gain along their mean free path, and that the lowest excitation energy E_a corresponds to the minima spacing extrapolated to $n = 0.5$, as shown in Figure 9.

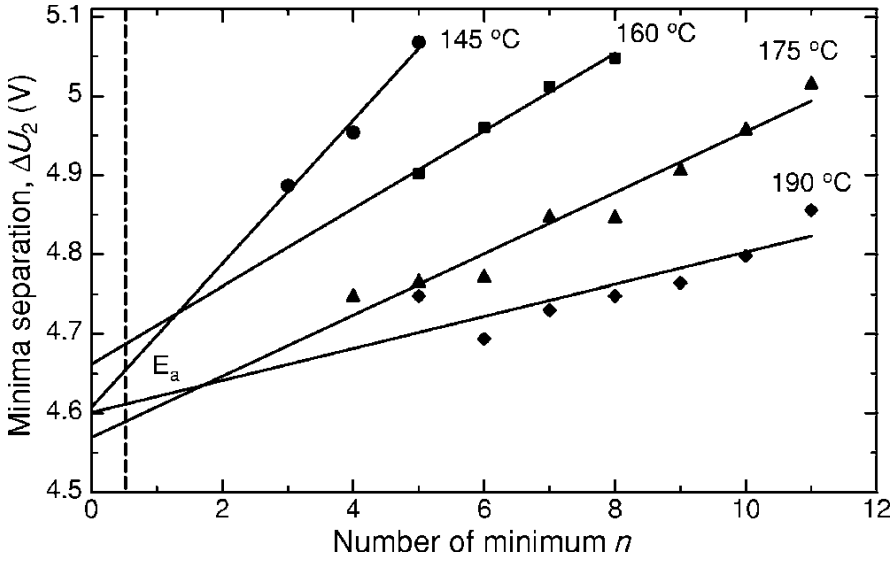

Figure 9 Spacing between minima in the Frank-Hertz experiment [7]. Measurements of the spacing between the n and $n-1$ minimums were made at four temperatures, and the linear fits (solid lines) are also shown.

Further, Rapior *et al*. go on to suggest that measuring the spacing between minima is more appropriate than measuring spacing between maxima of the oscillations. However, because measurements were taken at approximately 200℃, the variations in the maxima separation with peak number are small compared to voltage uncertainties, so using minima spacing would not likely have improved the results significantly. Nonetheless, future measurements should probably be done on the minima spacing, as indicated by Rapior *et al.* By taking so many peak measurements, the uncertainty was reduced by about 80% after taking the average period for each peak, but the accuracy and precision of the results could be improved by decreasing the step-size of the applied voltage. The quality (i.e. smoothness or noisiness) of the *I-V* characteristics is also dependent on vibrational motion of the experimental apparatus, so efforts should be made to reduce the amount of vibrations around the experiment.

Reducing the bias or retardation voltage between the grid anode and collector, thus increasing the collector potential, increased the overall magnitude of the anode current since the electrons are decelerated less or accelerated more between the grid and collector. On the other

hand, a positive bias voltage filtered out electrons with insufficient energy to pass through the retardation potential and reach the collector. At higher temperatures, the electrons have a smaller mean free path, so a lower bias voltage was required to allow the electrons to reach the collector, and higher anode voltages could be reached without igniting the mercury to produce several smooth oscillations. Additionally, as Figure 9 indicates, the spacing between peaks varies less with the peak number at higher temperatures. Conversely, low temperatures caused ignition of the mercury vapor around $V = 25\text{V}$ applied voltage and thus required a smaller filament current; the smaller filament currents results in fewer emitted electrons.

The monotonic rise in the current superimposed on the oscillations is due to the larger potential between the anode and cathode accelerating more electrons that do not necessarily collide with mercury atoms. Thus, an increasing number of electrons reach the collector as anode potential increases, increasing the overall anode current. As already indicated, the peaks in the *I*-*V* characteristic also do not have the same spacing. These effects may be reduced by changing the design of the vacuum tube parameters such as the mercury vapor density, and distance between the anode and cathode [3].

Summary

The work function for tungsten found using thermionic emission, $e\phi = 3.13 \pm 0.05$ eV, disagrees with the reference value of 4.5 eV for a typical tungsten filament. The linear fits had better reduced chi-squared values than those of the nonlinear fits, but both fit methods neglected uncertainties in the independent variables, which may have resulted in an underestimate in the fit parameter errors. Thus, an orthogonal distance regression may be a more appropriate fitting method in this case. In the Frank-Hertz experiment, the separation between *I*-*V* characteristic peaks depends on the peak number, so while the separation between some individual peaks

agreed with the theoretical excitation energy $\Delta E = 4.89$ eV, the average excitation energy $E_{\text{ex}} = 4.77 \pm 0.05$ eV disagrees. Better accuracy and precision in the measurement of the peak separation and thereby the excitation energy can be obtained by using smaller applied voltage step sizes.

References

[1] Frank-Hertz Experiment Lab Manual.
[2] G. P. Harnwell, J. J. Livinggood, *Experimental Atomic Physics* (McGraw-Hill, New York, 1933), p. 197-207.
[3] G. F. Hanne, *Am. J. Phys*. **56** (8), 696 (1988).
[4] A. C. Melissinos, *Experiments in Modern Physics*, (Academic Press, New York, 1966), p. 20.
[5] R. D. Larrabee, *J. Optical Am.* **49** (6), 619 (1959).
[6] CRC Handbook of Chemistry and Physics, 2012-2013.
[7] G. Rapior, K. Sengstock, V. Baev, *Am. J. Phys*. **74** (5), 423 (2006).